

Supplemental Information for Experimental Demonstration of Enhanced Photon Recycling in Angle-Restricted GaAs Solar Cells

Emily D. Kosten, Brendan M. Kayes, and Harry A. Atwater

1 The Modified Detailed Balance Model

To model the cells in our experiments, we utilized a modified detailed balance model, which included various forms of non-radiative recombination in addition to the radiative losses from the cell. This allows our model to be much more realistic than a traditional idealized detailed balance, where non-radiative losses are neglected. In addition, we simply input the measured short-circuit current, to avoid issues with the variability of the solar simulator lamp spectrum. Thus, the current at a given voltage, $J(V)$, in the modified model is expressed as:

$$J(V) = J_{sc} - \int_0^\infty [a(E) + n^2 a'(E)] \frac{2\pi q}{h^3 c^2} \frac{E^2}{e^{(E-qV)/kT} - 1} dE - qW(C_n n^2 p + C_p p^2 n) - 2qSp \quad (1)$$

where J_{sc} is the measured short-circuit current, and the rest of the terms give the various sources of loss from the cell. The first loss term includes radiative light emitted from the cell or absorbed in the back reflector, where $a(E)$ is the angle-averaged emissivity of the cell, and $a'(E)$ is the angle averaged absorption in the back reflector. n is the index of refraction in GaAs, and is included because light only needs to be emitted into the cell, rather than air, to

be absorbed in the back reflector [1, 2]. The next terms account for Auger recombination and surface recombination where C_n and C_p are the Auger coefficients [3], W is the cell thickness, and S is the surface recombination velocity, which we treat as an adjustable parameter. n and p , the electron and hole concentrations, are assumed to be constant across the cell and are determined from the assumed base doping, the neutrality condition, the cell voltage, and the law of mass action [4, 5].

We next develop an expression for $a'(E)$ and $a(E)$. Because these cell are relatively thick, we neglect modal structure within the cells, and utilize a multipass approach. For $a'(E)$ we consider separately light within the fused silica escape cone, and light that lies outside this escape cone. For light outside the escape cone, we extend Martí's approach and imagine light entering "through" the back reflector and then passing through the cell many times, being absorbed in both the cell and back reflector [1, 2]. The fraction of light absorbed in the back reflector is then expressed as:

$$a'(E, \theta) = \frac{(1 - R_b)(1 - e^{-2\alpha W / \cos \theta})}{1 - R_b e^{-2\alpha W / \cos \theta}} \quad (2)$$

where R_b is the reflectivity of the back reflector, α is the absorption coefficient of GaAs, and θ is the angle in GaAs. For light inside the escape cone, we use the same approach, but consider the reflectivity, R_c , and transmissivity, T_c , of the cell surface, to find the back reflector absorption:

$$a'(E, \theta) = \frac{(1 - R_b)(1 - T_c e^{-\alpha W / \cos \theta} - R_c e^{-2\alpha W / \cos \theta})}{1 - R_b R_c e^{-2\alpha W / \cos \theta}} \quad (3)$$

Finally, to calculate $a'(E)$ we evaluate $a'(E, \theta)$ for all angles, and take an angle average at each energy. We note that similar expressions have been derived by other authors for a perfectly absorbing back reflector, and that these expressions are a straightforward extension of the same approach. Furthermore, these results reduce to the previously derived results [1, 2].

To calculate the emissivity of the cell, $a(E)$, we use a multipass approach for light within the fused silica control or substrate. First, we find the fraction of light returned to the cell as a function of angle in the fused silica, ϕ , and the energy:

$$F_r(E, \phi) = \frac{R_t T_c}{1 - R_c R_t} \quad (4)$$

where R_t is the reflectivity at the top of the fused silica. For most angles, R_t is larger for the angle restrictor than the control, so more light will be returned and less light will ultimately escape the cell. Since light that is not recycled is ultimately emitted,

$$a(E, \theta) = (1 - F_r) a_c T_c n_g^2 \quad (5)$$

where we include the dual pass absorption of the cell, a_c , the transmissivity of the cell surface, and the fact that emission occurs into fused silica, with refractive index, n_g , rather than into air. Note that if the fused silica had an ideal AR coating, F_r would be zero and the emissivity would simply be a function of the cell absorption and surface reflectivity as we expect. Finally, we average the above expression over the angles in fused silica to find $a(E)$. (We could also do this calculation considering the angles in air rather than fused silica. While the result is the same with appropriate accounting of total internal reflection, we present the equations for fused silica as it is straightforward to generalize when accounting for light lost from the sides, as discussed below.)

When considering the side loss as in figure 4 of the main manuscript, our simple multipass expression for F_r is insufficient, as it neglects the cell edges. Therefore, we move to a ray-tracing model, where we incorporate the cell edges, cell mount, measurement stage, and the substrate geometry. In this ray tracing model, we place a source and receiver on the cell area, and find the fraction of rays returned to the cell as a function of wavelength and angle to determine F_r . We then proceed with the standard evaluation of $a(E)$ as above.

Once $a(E)$ is evaluated for each optical case, we use the measured Jsc and Voc values for

the control case to find a surface recombination velocity that describes the cell performance. Then, we use the fitted value of S along with the measured Jsc value and $a(E)$ for the angle restrictor to predict the Voc of the cell under angle restriction, as in figure 3 of the main manuscript. For figure 4 in the main manuscript, we simply include a separate set of ray trace derived $a(E)$ values for each optical setup. To determine the range for the calculation, we use the uncertainties in the Jsc and Voc, as determined from the multiple trials to determine a range for these values. We then use values for Jsc and Voc at the edges of the range along such that the value for S is maximized or minimized. Finally, we use these surface recombination values along with the observed temperature uncertainty and uncertainty in the measured Jsc to determine a range of values for the predicted Voc under angle restriction.

2 Rugate Angle Restrictor Design

As we noted in the main manuscript, one of the issues with the angle restrictor used in these experiments is the reduction in current due to reflections near normal incidence of 3-5%. Furthermore, a large second order reflecting band near 550nm would cause a very significant current loss if our spectrum were not filtered to only include light with wavelengths longer than 605nm. Thus, with the simplistic design used in the experiment, we would not expect any efficiency increase under the full solar spectrum even with a nearly ideal planar cell, as the current losses are too great. To achieve not only an increase in voltage, but also in overall performance, these current losses must be addressed. Here, we present a rugate or graded index design for angle restriction in GaAs, based on reference [6], which eliminates both the second-order reflecting band and the smaller ripple-type reflections near normal incidence observed in our experimental design [7, 8, 9]. While our experiment used an angle restrictor deposited on fused silica and compared to a bare piece of fused silica, here we design an angle restrictor to perform under glass, as in an installed solar array. Our concept is that

the angle restrictor would be deposited directly on the cell, with the glass covering attached with an index matched polymer to avoid any air gaps between the glass and angle restrictor. For a comparison case without angle restriction we consider a quintic-type graded index anti-reflection (AR) coating with the same index range and thickness as our angle restrictor deposited at the same glass/cell interface [10]. Thus, the performance of the graded index angle restrictor is compared to a graded index AR coating, assuming both are under glass.

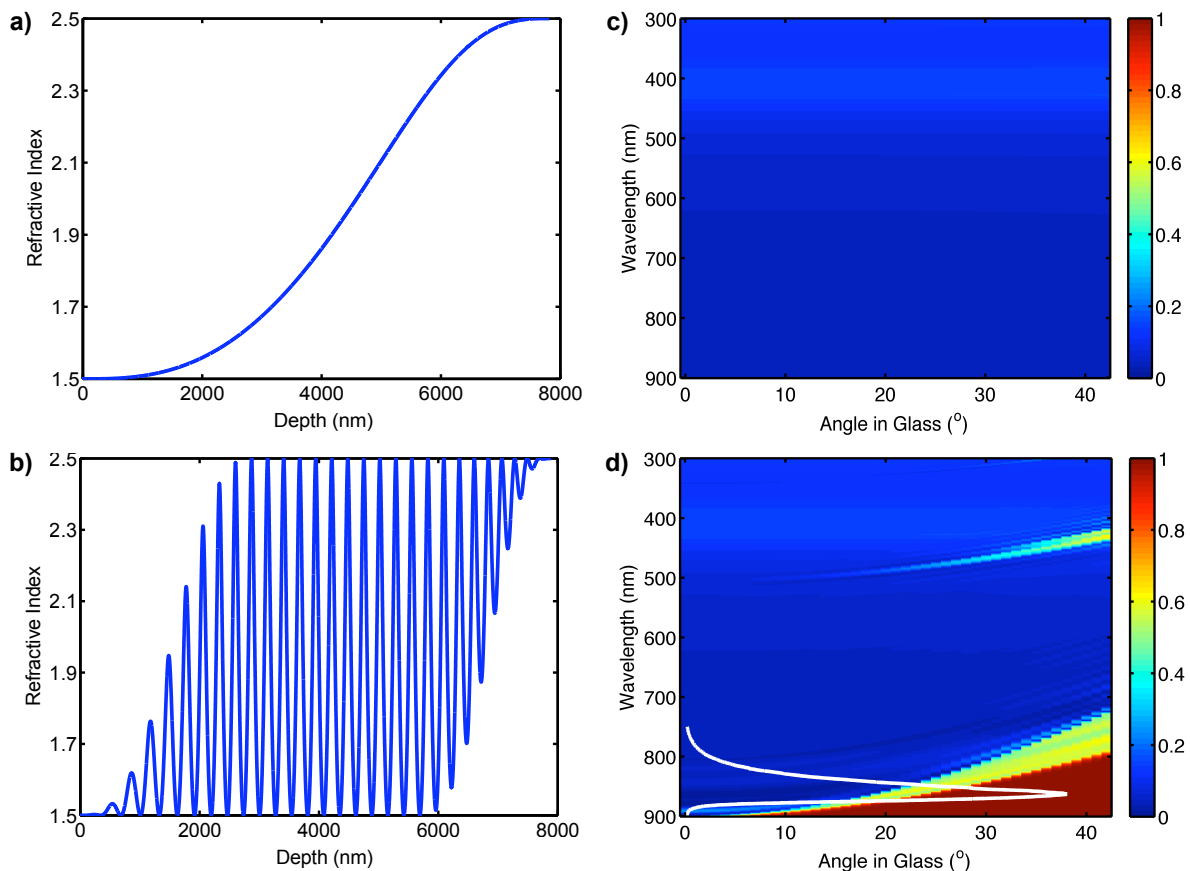


Figure 1: a) Refractive index profile of the graded-index AR coating used as a comparison case. Index range and optical thickness are matched to rugate angle restrictor. 0 represents the interface with the covering glass. b) Refractive index profile of rugate angle restrictor. 0 represents the interface with the covering glass. c) Calculated reflectivity values for the graded index AR coating comparison structure. Structure is assumed to be under glass and immediately above a GaAs cell with 20 nm AlInP window layer. d) Calculated reflectivity values for the rugate angle restrictor design. Structure is assumed to be under glass and immediately above a GaAs cell with 20 nm AlInP window layer. All calculations use the transfer matrix method with the rugate profile divided into 1 nm thick layers.

For this point design we assume the minimum refractive index in the rugate angle restrictor and graded index AR control is 1.5 and imagine a TiO₂/SiO₂ co-deposition process with a maximum index of 2.5 [11, 12, 13]. (We note that if high index TiO₂ cannot be achieved with co-deposition, similar increases in performance can be achieved with lower index TiO₂ films, though the currents and overall efficiencies are somewhat reduced for both the graded index AR control and the rugate angle restrictor due to increased reflection.) Figure 1 gives the refractive index profile and calculated reflectivity for both the graded index AR control and the rugate angle restrictor design [4, 14]. Unlike the simpler design used in the experiments, the rugate angle restrictor design has normal incidence transmission very similar to the graded index AR control and nearly complete suppression of the second-order reflecting band [6, 10]. Angle restriction to about 20 degrees is achieved near the peak in the emission spectrum, and, away from the angle restricting region, transmission is very similar for both the graded index AR control and the rugate angle restrictor across all angles. Thus, for most of the spectrum, diffuse light should be utilized equally well for the angle restrictor and graded index AR coating.

To quantify this further, in figure 2 we estimate the short-circuit current in the cell as a function of the light incidence angle based on the cell internal quantum efficiency (IQE) spectrum and the transmission spectrum, including reflections from the top surface of the glass. The predicted current with the rugate angle restrictor is 99.98% of the graded-index AR comparison value at normal incidence, and remains above 99% up to 25 degrees. Furthermore, the minimum current with the rugate angle restrictor at any angle is 77% of the graded index AR control value, so we expect a large portion of the diffuse light to be captured with this design.

Next, we evaluate the efficiencies of cells with the graded index AR control and rugate angle restrictor using the modified detailed balance model with short-circuit current values from figure 2. We use a multipass model to account for reflections between the cell/glass interface, where the rugate angle restrictor or graded index AR is deposited, and the glass/air

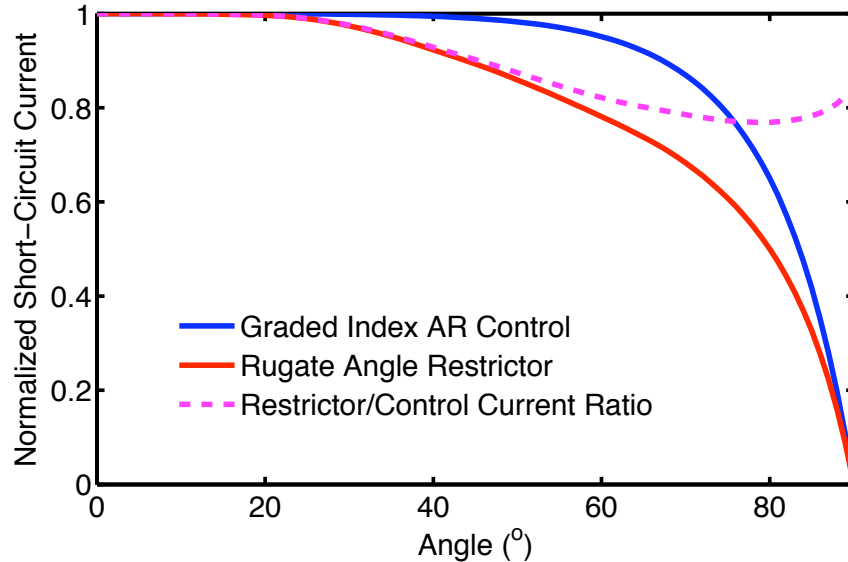


Figure 2: Predicted J_{sc} as a function of light incidence angle for the rugate angle restrictor (red line) and graded index AR control (blue line) structures under glass. Values are normalized to the graded index AR structure at normal incidence. The ratio of the J_{sc} values is also plotted (dotted purple line).

interface. As in figure 3, we vary the surface recombination velocity S , assuming an ideal back reflector, thereby varying the ERE up to the Auger limit. However, as the Auger limit is dependent on cell thickness and doping, we also perform the calculation at 100% ERE. As we expect, for higher ERE cells there is a larger improvement in efficiency with angle restriction. As shown in figure 3, for this point design we expect a 1% relative efficiency increase for cells with ERE values corresponding to the current GaAs world record [15], and a 2.5% relative efficiency increase for Auger limited cells with a 27mV V_{oc} enhancement.

Because of this design's wide acceptance angle, it can also be used under a conventional concentrator, rather than to collect diffuse light. Because currents are maintained out to 25 degrees, we assume a conventional concentrator with an input angle of 2 degrees, and an output angle of 25 degrees, operating at the thermodynamic concentration limit of 146.6 suns [16]. We further assume that light output from the concentrator is evenly distributed over the angular range from 0 to 25 degrees, and determine the predicted current and efficiency for the cell. As in figure 4, at low ERE values current losses from the wide range of input

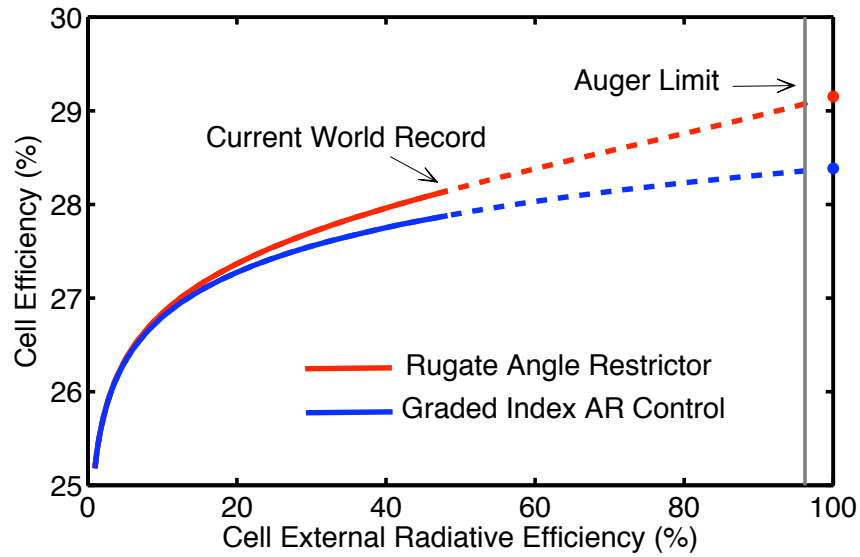


Figure 3: Predicted efficiency as a function of external radiative efficiency for the rugate angle restrictor (red) and the graded-index AR control (blue). The solid line indicates the range ERE values attainable with current GaAs cells. The end of the solid line corresponds approximately to ERE values for current world record cells [15]. The dotted line indicates ERE values beyond current world record cells and terminates at the Auger limit (grey line). Finally, the dots indicate efficiency values at the radiative limit (ERE=100%). Note that in the ERE range considered experimentally (3-16%) the angle restrictor and control lines are nearly overlaid, indicating a small voltage enhancement with angle restriction in this region, similar to the voltage enhancement we observed experimentally.

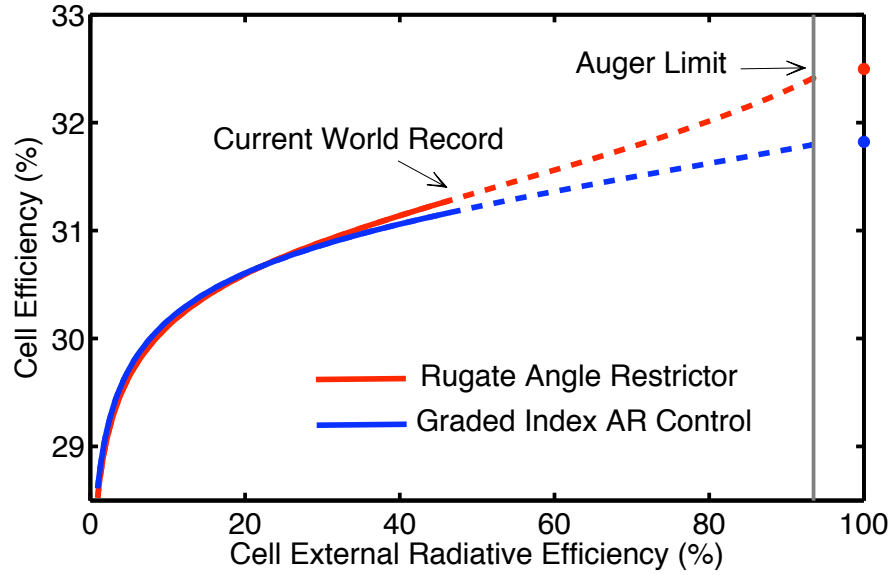


Figure 4: Predicted efficiency as a function of external radiative efficiency for the rugate angle restrictor (red) and the graded index AR control (blue) under a 146.6x concentrator with 25 degree output angle. The solid line indicates the range ERE values attainable with current GaAs cells. The end of the solid line corresponds approximately to ERE values for current world record cells at one sun.[15] The dotted line indicates ERE values beyond current world record cells and terminates at the Auger limit (grey line). Finally, the dots indicate efficiency values at the radiative limit (ERE=100%).

angles outweigh voltage gains, and efficiencies are slightly reduced with angle restriction. However, with a high ERE cell, efficiency gains with angle restriction are possible under fairly high concentrations.

3 Bandgap Raising and Angle Restriction Effects

For a cell with suitably high ERE, placing an omnidirectionally reflecting structure on the cell to completely block emitted light can lead to an effective “photonic” increase in the cell bandgap [17, 18]. While we intentionally designed our angle restricting structure to not block normal incidence light above the cell bandgap, the angle restrictor as-deposited had an approximately 25 nm blue shift in the normal incidence transmission cut-off. Thus, some of the voltage increase observed may be due to this band-gap raising effect rather than a pure angle restriction effect. To quantify this, we calculated the expected voltage increase for the highest ERE cell for both the as-deposited angle restrictor and the angle restrictor as it was originally designed, using the calculated reflectivity values. For the designed angle restrictor, we predict a current-normalized Voc increase of 3.3mV, as opposed to the 4.0mV prediction for the measured reflectivity values. Thus, angle restriction is clearly the dominant effect. In addition, we modeled the effect of an ideal bandgap-raising reflector for cells of similar ERE to those used in these experiments. We found that Voc actually decreased with the bandgap-raising reflector, as the losses in Jsc from the reflector were not offset by the reduction dark current with enhanced photon recycling. While the departures from the original design have some impact on the voltage increase we observe, bandgap raising alone could not produce the Voc effect we observe in cells of this radiative quality, and angle restriction is the primary effect.

4 Materials and Methods

4.1 Cell Contacting and Characterization

High efficiency 1 cm² GaAs solar cells were provided by Alta Devices. To eliminate variability associated with probe based contacting, permanent silver ribbon (E. Jordan Brooks Solar) based contacts were installed on the cells using a silver epoxy (Epotek H20F) with a surrounding dielectric epoxy to prevent shorting (Creative Materials 119-48). Photoluminescence (PL) spectra were taken at room temperature in a Zeiss Axio Observer inverted microscope with a 10x objective with illumination from a 630nm pulsed diode laser. The photoluminescence emission was spectrally resolved with a Roper Scientific CCD (Model 7346-0001) and a Princeton Instruments Acton SP2150 monochromator. The PL curves shown in figures 1c and 1d weight the raw photoluminescence spectra with external quantum efficiency data provided by Alta Devices to eliminate sub-band defect mediated photoluminescence, which cannot be usefully recycled.

4.2 Optical Coupler Fabrication and Characterization

The angle restricting dielectric multilayer was designed and modeled with a transfer matrix method approach using the OpenFilters program [19]. The dielectric multilayer design was deposited on 2.2mm thick fused silica substrates by Reynard Corp., who also provided refractive index information for their materials. The angle dependent reflectivity spectra were taken in a home-built integrating sphere setup utilizing a Fianium white light laser source with a monochromator. In order to measure the dielectric coated interface most directly, the measurements were taken from air. Owing to errors in the measurement, a few data points gave reflectivity values slightly greater than one. These points were set to one and the reflections on the back surface of the substrate were subtracted. To subtract the back surface reflections, a multipass approach was utilized, with reflections at the back surface of the fused silica determined from the Fresnel equations and the refractive index of fused

silica. The measured reflectivity in the integrating sphere includes both the reflectivity of the dielectric on the first pass and the reflection of transmitted light from the back surface that is subsequently transmitted through the dielectric. Accounting for the multiple passes of transmitted light in the fused silica we find that the measured reflectivity, R_m , is:

$$R_m = R_d + \frac{T_d^2 R_b}{1 - R_b R_d} \quad (6)$$

where R_d and T_d are the reflection and transmission at the dielectric coated surface, and R_b is the reflection at fused silica-air interface at the back of the substrate. All reflection and transmission values are refer to a given angle in air and the corresponding angle in fused silica, as determined by Snell's law. Re-arranging the above expression gives:

$$R_d = \frac{R_m - R_b}{1 - 2R_b + R_m R_b} \quad (7)$$

The resulting values of R_d are plotted in figure 1d and were used to calculate the angle restrictor emissivity for the detailed balance model. For the purposes of calculating emissivity, reciprocity allows us to equate R_d at a given angle in air with R_d at the corresponding angle in fused silica, as determined from Snell's law. Fused silica substrates for use as controls were obtained from Reynard Corp. To eliminate side loss, the substrates were scribed and broken to approximately 13 mm x 12 mm. Side reflectors consisting of an 2 nm Cr adhesion layer and 400 nm of gold were deposited in an AJA magnetron sputtering system under DC power.

4.3 Current-Voltage Measurements

Angle restrictor and control optics were coupled to the cells using Cargille Fused Silica Index Matching Liquid (50350) at the interface of the cell and the fused silica substrate. Dark current measurements were performed using a Keithley 238 high current source measure unit. Dark current fits assumed a temperature of 24 °C, and were performed in Matlab

using least-squares curve fitting with the Levenberg-Marquardt algorithm.

All light IV measurements were performed under an ABET Technologies solar simulator with 1° angular spread calibrated to 100 mW/cm². The spectrum was filtered using a Chroma Technologies (ET605LP) long pass filter with a 605 nm cutoff. The cells were measured on a temperature controlled stage, and were allowed to cool for three minutes between each IV sweep. However, peak stage temperature variations of approximately 0.1 °C were observed. IV sweeps were taken with a Keithley 2440 5A SourceMeter. Five sweeps were taken for each configuration with the standard deviation defining the error in Voc and Jsc. For the solar simulator adjustments necessary to equalize the currents, the precise concentrations are not known, but currents to the solar simulator lamp were increased by 1-1.5 A depending on the cell, over a base value of 48.1 A.

4.4 Implementation of the Modified Detailed Balance Model

To model the voltage increase we use the modified detailed balance model implemented in Matlab. Based on observed peak stage temperatures, all simulations assumed 299 K. To determine ERE for each cell, we fit the surface recombination velocity to match the measured Voc under the control optic with the measured Jsc under the control. Taking the ratio of the radiative emission relative to all recombination at Voc gave the ERE value reported in figure 3. Fitted surface recombination velocity (SRV) values ranged from 591 to 2410 cm/sec. Differences in back reflector type, and material quality, as reflected in the effective SRV values, lead to the variations in ERE across the four cells in figure 3. The experiments in figures 2 and 4 utilized the 15.7% ERE cell reported in figure 3. Auger recombination assumed 1×10^{17} n-type GaAs [4]. Back reflector losses were calculated using the Fresnel equations. To find the emissivity at each wavelength and angle, we used a multipass model assuming the light bounces between the cell and the fused silica/air top interface with no other sources of loss (see SI). The reflectivity of the top surface with the angle restrictor was derived from integrating sphere measurements as described above, and was calculated

using the Fresnel equations for the fused silica control. The reflectivity at the cell surface was found using the transfer matrix method, assuming a 20 nm AlInP window layer, based on NREL designs.[4] For the AR coated (15.7% ERE) cell, we assumed 50 nm of TiO₂ and 100 nm of SiO₂ above the window layer.

4.5 Gradual Coupling Measurements

For the gradual coupling experiments in figure 4, cylinders of the varying heights were assembled from 25 mm diameter fused silica substrates of 2.2 mm and 6 mm thickness, provided by Reynard corporation. Cargille fused silica index matching liquid was used between the cell-fused silica and fused silica-fused silica interfaces. All substrates had ground glass edges, and currents were equalized across all configurations by adjusting the solar simulator as necessary. While the precise solar concentrations of this adjustment are not known, the currents to the simulator lamp ranged from 47.0 A for the control case to 48.7 A for the tallest restrictor structure. The modified detailed balance model was used with a ray trace to find the emissivity. The ray trace was performed in LightTools, a commercial software. The ground glass edges were assumed to be Lambertian surfaces, with reflectivity based on total internal reflection and Fresnel losses. For the ray trace, the reflectivity spectrum of the material surrounding the cell was measured in the Zeiss Axio Observer setup utilized for PL measurements, but with a lamp source. The gold edge reflectivity was modeled for the ray trace using the transfer matrix method assuming a 2 nm Cr layer with an optically thick Au layer.

References

- [1] O.D. Miller, E. Yablonovitch, and S.R. Kurtz. Strong internal and external luminescence as solar cells approach the Shockley-Queisser limit. *IEEE J. of Photovoltaics*, 2:303–311, 2012.

- [2] A. Martí, J.L. Balenzategui, and R.F. Reyna. Photon recycling and Shockely's diode equation. *J. Appl. Phys.*, 82(8):4067–4075, 1997.
- [3] U. Strauss, W. W. Ruhle, and K. Kohler. Auger recombination in intrinsic GaAs. *Appl. Phys. Lett.*, 62(55), 1993.
- [4] M.A. Steiner, J.F. Geisz, I. García, D.J. Freidman, A. Duda, and S.R. Kurtz. Optical enhancement of the open-circuit voltage in high quality GaAs solar cells. *J. Appl. Phys.*, 113:123109, 2013.
- [5] S.M. Sze and K.K. Ng. *Physics of Semiconductor Devices*. Wiley-Interscience, 1998.
- [6] S. Fahr, C. Ulbrich, T. Kirchartz, U. Rau, C. Rockstuhl, and F. Lederer. Rugate filter for light-trapping in solar cells. *Opt. Exp.*, 16(13):9332–9343, 2008.
- [7] C. Ulbrich, S. Fahr, J. Upping, M. Peters, T. Kirchartz, C. Rockstuhl, R. Wehrspohn, A. Gombert, F. Lederer, and U. Rau. Directional selectivity and ultra-light-trapping in solar cells. *Phys. Stat. Sol. A*, 205(12):2831–2843, 2008.
- [8] B. G. Bovard. Rugate filter theory: an overview. *Appl. Opt.*, 32(28):5427–5442, 1993.
- [9] W. H. Southwell. Using apodization functions to reduce sidelobes in rugate filters. *Appl. Opt.*, 28(23):5091–5094, 1989.
- [10] W. H. Southwell. Gradient-index antireflection coatings. *Opt. Lett.*, 8(11):584–586, 1983.
- [11] W. J. Gunning, R. L. Hall, F. J. Woodberry, W. H. Southwell, and N. S. Gluck. Codeposition of continuous composition rugate filters. *Appl. Opt.*, 28(14):2945–2948, 1989.
- [12] J.-S. Chen, S. Chao, J.-S. Kao, H. Niu, and C.-H. Chen. Mixed films of TiO₂—SiO₂ deposited by double electron-beam coevaporation. *Appl. Opt.*, 35(1):90–96, 1996.

- [13] H. Demiryont. Optical properties of SiO₂-TiO₂ composite films. *Appl. Opt.*, 24(16):2647–2650, 1985.
- [14] S.J. Orfanidis. *Electromagnetic Waves and Antennas*. 2010. (www.ece.rutgers.edu/~orfanididi/ewa/).
- [15] Brendan Kayes. personal communication.
- [16] W.T. Welford and R. Winston. *High Collection Nonimaging Optics*. Academic Press, 1989.
- [17] A. Niv, Z. R. Abrams, M. Gharghi, C. Gladden, and X. Zhang. Overcoming the bandgap limitation on solar cell materials. *Appl. Phys. Lett.*, 100(8):083901, 2012.
- [18] J. N. Munday. The effect of photonic bandgap materials on the shockley-queisser limit. *J. Appl.Phys.*, 112(6):064501, 2012.
- [19] S. Larouche and L. Martinu. Openfilters: open-source software for the design, optimization, and synthesis of optical filters. *Appl. Opt.*, 47(13), 2008.